EDGE ARTICLE

CrossMark
click for updates

Precious-metal free photoelectrochemical water splitting with immobilised molecular Ni and Fe redox catalysts†

Timothy E. Rosser, Manuela A. Gross, Yi-Hsuan Lai and Erwin Reisner*

Splitting water into hydrogen and oxygen with molecular catalysts and light has been a long-established challenge. Approaches in homogeneous systems have been met with little success and the integration of molecular catalysts in photoelectrochemical cells is challenging due to inaccessibility and incompatibility of functional hybrid molecule/material electrodes with long-term stability in aqueous solution. Here, we present the first example of light-driven water splitting achieved with precious-metal-free molecular catalysts driving both oxygen and hydrogen evolution reactions. Mesoporous TiO_2 was employed as a low-cost scaffold with long-term stability for anchoring a phosphonic acid-modified nickel(II) bis-diphosphine catalyst (**NiP**) for electrocatalytic proton reduction. A turnover number of 600 mol H_2 per mol **NiP** was achieved after 8 h controlled-potential electrolysis at a modest overpotential of 250 mV. X-ray photoelectron, UV-vis and IR spectroscopies confirmed that the molecular structure of the Ni catalyst remains intact after prolonged hydrogen production, thereby reasserting the suitability of molecular catalysts in the development of effective, hydrogen-evolving materials. The relatively mild operating conditions of a pH 3 aqueous solution allowed this molecule-catalysed cathode to be combined with a molecular Fe(II) catalyst-modified WO_3 photoanode in a photoelectrochemical cell. Water splitting into H_2 and O_2 was achieved under solar light illumination with an applied bias of >0.6 V, which is below the thermodynamic potential (1.23 V) for water splitting and therefore allowed the storage of solar energy in the fuel H_2.

Introduction

Splitting water into hydrogen and oxygen using insolation, a process considered as 'artificial photosynthesis', is viewed as a promising sustainable solution to meeting the increasing global demand for transportable fuel and storable renewable energy. The reliance on the long excited state lifetimes[1] and excellent catalytic properties[2,3] characteristic of components based on low-abundance precious metal elements such as Ru and Pt remains a barrier to low-cost water splitting.[4,5] Consequently, only a handful of systems that achieve full water splitting make use of catalysts made from only Earth-abundant elements.[6–8] Of these, none rely on synthetic molecular catalysts driving both the H_2 and O_2 evolution half reactions, and as such the realisation of this goal remains a significant challenge.[9,10]

The specific interest in molecular catalysts arises from the precise control afforded by modern synthetic chemistry over the individual catalytic centres, and therefore the opportunity to study the chemical and structural influences on catalysis.[11–13] Indeed, there have been cases where only molecular catalysts, and not noble metal nanoparticles, are found to perform H_2 evolution.[14] Thus far, H_2 evolution with molecular catalysts driving the reduction and oxidation reactions in homogeneous solution has only been achieved in the context of oxidation of an organic substrate.[15,16] Thus, homogeneous approaches have failed to date in demonstrating full splitting of H_2O into H_2 and O_2.

A photoelectrochemical (PEC) approach to water splitting utilising immobilised molecular catalysts has many advantages. It allows efficient use of highly active and selective catalytic centres ('single-site-catalysis'), can overcome kinetic restrictions from diffusion limitations, separates the redox half-reactions to avoid quenching mechanisms and allows separation of the gaseous products, as well as providing a platform for the systematic study of molecular catalysts under aqueous conditions without the requirement of water-solubility.[11,17] Recently, the first molecule-catalysed tandem PEC cells with an immobilised Co-based catalyst driving a dye-sensitised NiO photocathode and a Ru catalyst on a dye-sensitised photoanode have demonstrated full water splitting.[18,19] However, this PEC cell

Christian Doppler Laboratory for Sustainable SynGas Chemistry, Department of Chemistry, University of Cambridge, Lensfield Road, Cambridge CB1 2EW, UK. E-mail: reisner@ch.cam.ac.uk; Web: http://www-reisner.ch.cam.ac.uk

relies on a precious metal (Ru) water oxidation catalyst and the lability of the axial pyridine on the cobalt H_2 evolution catalyst limits the long-term applicability of the H_2-evolving photocathode.

In this study, we present the first example of molecular catalyst-enabled water splitting using only Earth-abundant elements (Scheme 1). We have selected the Ni(II) bis-diphosphine class of H_2 evolution catalyst due to its high activity in both aqueous[20,21] and non-aqueous[22] conditions and lack of a labile ligand that could undergo hydrolysis or displacement during catalysis, and immobilised a phosphonate-bearing example on a mesoporous TiO_2 electrode. We have studied the activity and stability of this hybrid cathode, finding both to be excellent in mild aqueous conditions, which are essential for combination with a photoanode for solar water splitting. An Fe(II)-based molecular catalyst immobilised on WO_3 has shown a well-characterised increase in activity and selectivity for O_2 evolution in mildly acidic aqueous conditions compared to the unmodified electrodes,[23] and as such was have combined the TiO_2 hybrid cathode with a Fe-catalyst modified WO_3 photoanode in a PEC water splitting cell.

Results and discussion

Hybrid H_2 evolution cathode

Ni(II) bis(diphosphine) complexes are a family of bio-inspired proton reduction catalysts,[22,24,25] and the phosphonate-bearing catalyst **NiP** (Scheme 1) ranks among the most active precious-metal free molecular H_2 evolution catalysts in aqueous conditions.[14,20,26] **NiP** was reported with turnover numbers (TONs) in excess of 700 mol H_2 per mol **NiP** in photocatalytic schemes using a Ru(II)-based dye and ascorbic acid as an electron donor, and has been demonstrated as a homogeneous electrocatalyst in pH 4.5 aqueous solution.[27] **NiP** features phosphonic acid groups, which are well-established for effective binding to TiO_2 under mildly acidic aqueous conditions,[28–30] through a variety of modes such as P–O–Ti and hydrogen bonding, depending on the exposed TiO_2 facet.[31] These anchoring groups and the low ligand lability of **NiP** make it an ideal candidate for

immobilisation on metal oxide electrodes for single-site heterogeneous proton reduction.

Attachment of molecular H_2-evolving catalysts bearing phosphonic acid groups to metal oxides in acidic and pH neutral conditions has been demonstrated,[20,32] including the electrochemical reduction of aqueous protons with cobalt(III) catalysts immobilised onto mesoporous indium-doped tin oxide (ITO) electrodes.[11,33] The performance of these electrodes, however, was low due to instability of ITO under reducing conditions, as well as the intrinsically low stability of the cobalt catalyst during turnover. **NiP** displays substantially higher activity than the previously employed Co-based catalysts and we replaced the electrodegrading ITO cathode with robust TiO_2. Although TiO_2 is often considered as a classical insulator and therefore unsuitable as electrode material, it has previously been used for electrocatalytic proton reduction with immobilised H_2-cycling enzymes known as hydrogenases,[34,35] and we aim here to establish its use as an electrode substrate for synthetic molecular catalysts such as **NiP** for long-term reductive electrocatalysis.

NiP was synthesised and characterised as described previously,[20] and mesoporous TiO_2 (mesoTiO_2) electrodes were prepared by doctor blading a suspension of P25 TiO_2 (8 : 2 anatase : rutile ratio, 25 nm average particle size) onto an FTO-coated glass substrates, followed by annealing at 450 °C. MesoTiO_2 electrodes with a geometrical surface area of 1.0 cm^2 were employed and scanning electron microscopy (SEM) revealed a film thickness of 4 μm (Fig. S1†). Modification with **NiP** was achieved by submersion of mesoTiO_2 in a methanol solution of the Ni(II) compound (0.5 mM) for 18 h at room temperature, followed by rinsing with methanol and drying under a stream of N_2. The amount of **NiP** per geometric surface area of the TiO_2 electrode was determined as 14.6 ± 2.0 nmol cm^{-2} by spectrophotometry (at λ_{abs} = 257 and 300 nm) following desorption of the catalyst from TiO_2 with aqueous NaOH (0.1 M). The loading of **NiP** is in agreement with previous results, where a surface coverage of 53 nmol cm^{-2} was observed for a phosphonic acid-modified ruthenium complex on 10 μm thick mesoporous TiO_2 electrodes.[36]
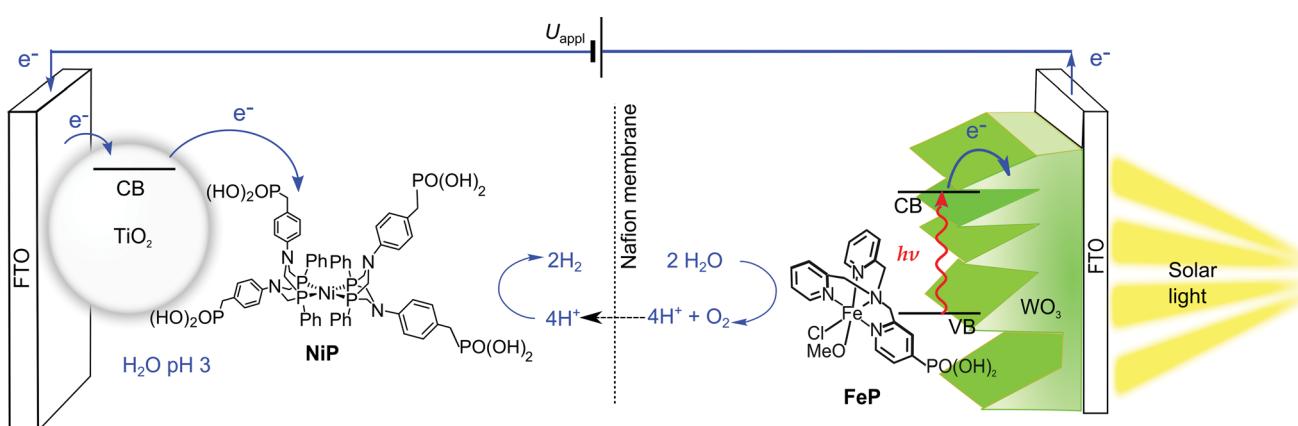
Scheme 1 Schematic representation of PEC water splitting with the TiO_2|**NiP** hydrogen evolution cathode wired to the WO_3|**FeP** oxygen evolution photoanode in an aqueous electrolyte solution at pH 3.

Cyclic voltammograms (CVs) of the resultant **NiP**-modified mesoTiO$_2$ (TiO$_2$|**NiP**) electrodes and bare mesoTiO$_2$ in aqueous pH 3 electrolyte solution (0.1 M Na$_2$SO$_4$) are shown in Fig. 1a, and suggest H$_2$ evolution activity of the immobilised Ni(II) catalyst. The CVs of the unmodified TiO$_2$ electrode show a typical 'trumpet plot' response as expected for a semiconductor electrode.[37] The reductive current observed upon the cathodic scan ($Q = -0.6$ mC at $\nu = 100$ mV s^{-1}), with an onset of approximately -0.1 V *vs.* the reversible hydrogen electrode (RHE), was followed by an oxidising current ($Q = +0.4$ mC) in the anodic scan. This observation was attributed to filling and emptying of the conduction band (CB) of TiO$_2$. At pH 3, after modification with **NiP**, the oxidative current in the anodic scan is substantially diminished, with the charge ratio for the cathodic to anodic scans higher than 15 : 1, consistent with the consumption of the electrons from the CB of TiO$_2$ for proton reduction catalysis.

Evidence that the electrons are transferred to the catalyst *via* the CB of TiO$_2$ was obtained by spectroelectrochemistry.[38] When an applied potential, E_{appl}, of -0.43 V *vs.* RHE was applied to TiO$_2$ electrodes, a blue colour was observed, and the corresponding increase in absorbance between 600 and 900 nm in the UV-vis spectrum is shown in Fig. S2a.† We assigned this absorption to d–d transitions in Ti^{3+}, which is formed by filling the CB of TiO$_2$.[39,40] When treated with **NiP**, the increase in absorbance between 600 and 900 nm was still observed at $E_{appl} = -0.43$ V *vs.* RHE (Fig. S2b†), but to a lesser extent, due to a lower steady-state concentration of electrons in the CB. To study the release of CB electrons to **NiP**, the time-resolved absorbance[38] of an unmodified and **NiP**-modified mesoTiO$_2$ electrode was monitored at $\lambda = 800$ nm with $E_{appl} = -0.43$ V *vs.* RHE for 20 s, followed by a return to no applied potential

(Fig. 1b). In the absence of **NiP**, the CB electrons are only slowly released from TiO$_2$ after charging at -0.43 V *vs.* RHE, which is consistent with the oxidising (discharging) current observed in the return scan of the CV in Fig. 1a. In the presence of **NiP** on mesoTiO$_2$, the absorbance at $\lambda = 800$ nm decayed to its original value within a few seconds ($\tau_{1/2} = 2.3$ s) of the potential being removed, supporting the efficient release of CB electrons to **NiP**.

Sustained electrocatalytic H$_2$ production by the TiO$_2$|**NiP** cathode was confirmed by controlled-potential electrolysis (CPE) in pH 3 aqueous electrolyte solution, and the amount of H$_2$ produced alongside the theoretical maximum (assuming 100% faradaic efficiency) is shown in Fig. 2a. MesoTiO$_2$ electrodes modified with **NiP** were held at $E_{appl} = -0.25$ V *vs.* RHE in a two-compartment electrolytic cell for 8 h, during which time a charge of 2.02 ± 0.17 C passed. The current decayed slowly during the first few hours, which is consistent with the good stability of the molecular catalyst in aqueous solution (Fig. S3a†).[20,27] Analysis of the headspace of the electrochemical cell by gas chromatography revealed that 9.26 ± 2.1 μmol of H$_2$ was produced after 8 h, which corresponds to a faradaic yield of $88 \pm 17\%$ and a Ni-based turnover number with a lower limit of 600 (assuming that all **NiP** remained electroactive on the electrode during CPE).

The fraction of adsorbed catalyst and molecular integrity were study by UV-vis absorption spectroscopy after electrolysis. **NiP** was desorbed from mesoTiO$_2$ with NaOH (0.1 M) after 8 h CPE and the UV-vis spectrum of the resultant solution matched a reference spectrum recorded from freshly-modified electrodes treated in the same way, suggesting minimal degradation of the ligand framework of **NiP** (Fig. S4a†). The loading of **NiP** after CPE was 10.9 ± 2.5 nmol cm^{-2}, which corresponds to 75% of that measured on the freshly-modified electrodes, thus demonstrating strong attachment between the phosphonate anchor and the TiO$_2$ surface even under reducing conditions.
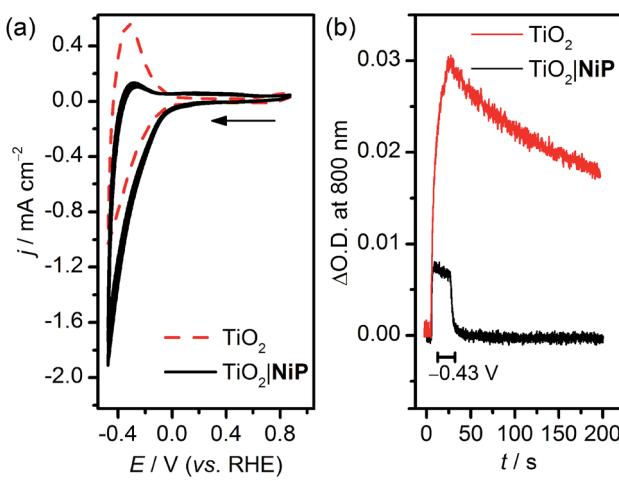
Fig. 1 (a) CVs of **NiP** immobilised on mesoTiO$_2$ (solid black line, TiO$_2$|**NiP**) and unmodified mesoTiO$_2$ (dashed red line) performed at $\nu = 100$ mV s^{-1} (the arrow indicates the start of the experiment). (b) Spectroelectrochemistry of the same electrodes monitoring the absorbance change (ΔO.D.) at $\lambda = 800$ nm before (no applied potential), during CPE at $E_{appl} = -0.43$ V *vs.* RHE for 20 s (starts at 6 s), and following CPE (no applied potential). Conditions: a Ag/AgCl reference electrode and a Pt mesh counter electrode in aqueous Na$_2$SO$_4$ (0.1 M) solution at pH 3, N$_2$ atmosphere and room temperature.
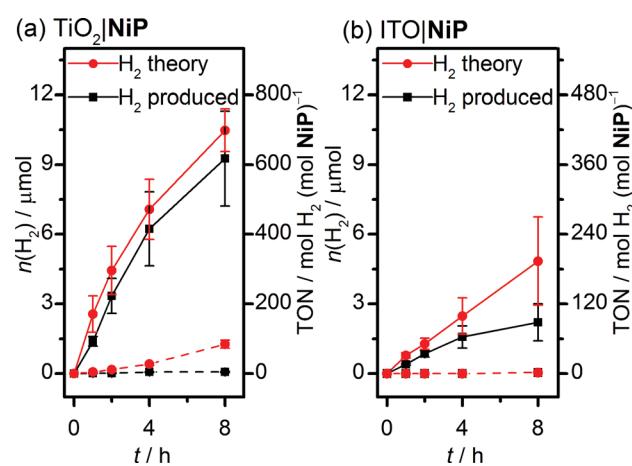
Fig. 2 Amount of H$_2$ generated over time during CPE of **NiP**-modified (solid line) and unmodified (dashed line) with (a) mesoTiO$_2$ and (b) mesoITO electrodes at $E_{appl} = -0.25$ V *vs.* RHE. The theoretical amount of H$_2$ was calculated based on 100% faradaic yield and the experimentally produced H$_2$ was quantified by gas chromatography. Conditions: a Ag/AgCl reference electrode and a Pt mesh counter electrode in aqueous Na$_2$SO$_4$ (0.1 M) solution at pH 3, N$_2$ atmosphere and room temperature.

Further evidence for the retention of molecular **NiP** after CPE was obtained by attenuated total reflectance Fourier transform infrared (ATR-FTIR) spectroscopy. Fig. S4b† shows the FTIR spectra of **NiP** powder, TiO$_2$|**NiP** before and after 4 h CPE at -0.25 V *vs.* RHE, and TiO$_2$ (treated with Na$_2$SO$_4$ electrolyte solution). Stretches at 1260 cm^{-1} (P=O), 1440 and 1510 cm^{-1} (**NiP** ligand) were present in the reference **NiP** spectrum and TiO$_2$|**NiP** before and after CPE, but not the TiO$_2$ background, reasserting the molecular integrity of the catalyst surviving many turnovers on the electrode surface.

MesoTiO$_2$ displayed substantially improved performance to mesoITO, which has previously been used as a substrate for a phosphonate-bearing Co-based catalyst.[33] We prepared mesoporous ITO electrodes (for synthetic details see the Experimental section) with a **NiP** loading per geometric surface area of 25 nmol cm^{-2}. Although the CV supports a catalytic current for ITO|**NiP** in an aqueous pH 3 electrolyte solution (Fig. S5†), CPE at $E_{appl} = -0.25$ V *vs.* RHE (Fig. S3b†) shows the formation of only 2.2 ± 0.8 µmol of H$_2$ after 8 h with a faradaic efficiency of $49 \pm 14\%$ (Fig. 2b). The low faradaic efficiency is attributed to competing reductive degradation of the ITO, thus demonstrating the fragility of the ITO electrodes under reducing conditions compared with TiO$_2$.

Electrocatalytic activity of TiO$_2$|**NiP** was highest at pH 3 and a lower performance was observed in electrochemical experiments in pH 4 and pH 2 electrolyte solutions. The CV of TiO$_2$|**NiP** at pH 4 is shown in Fig. S6a† and it does not display the same loss of oxidative discharging of the CB as observed at pH 3 (Fig. 1a). This implies loss of performance, which is corroborated by a lower H$_2$ production rate during CPE at $E_{appl} = -0.33$ V *vs.* RHE (Fig. S6b†). When electrolysis was performed at pH 2 under otherwise the same conditions, activity was again observed to be lower than at pH 3 (Fig. S5†), establishing pH 3 aqueous solution as an optimum for TiO$_2$|**NiP**. This optimum pH for TiO$_2$|**NiP** is in agreement with the previously reported higher electrocatalytic activity of **NiP** in pH 3 compared to pH 4 in homogeneous solution.[20] The pendant amines in **NiP** have a pK_a of approximately 3,[41] suggesting this to be the optimum pH for proton transfer to the Ni centre, which is a key mechanistic feature of this class of catalyst.[22]

We have also tested the influence of O$_2$ on the activity of TiO$_2$|**NiP** as O$_2$ tolerance is an important property for a proton reduction catalyst in water splitting.[27,42,43] The H$_2$ production activity by the TiO$_2$|**NiP** cathode was found to be less effective in a pH 3 electrolyte solution under an atmosphere of air, compared to when purged with N$_2$ as presented above. When subjected to CPE at $E_{appl} = -0.25$ V *vs.* RHE for 4 h under air, the TiO$_2$|**NiP** retained only some activity (Fig. S7†), achieving a TON of 39 ± 16 but with a low faradaic efficiency of 7%. This significant drop in activity in the presence of oxygen corroborates a similar deactivation observed for **NiP** in homogeneous aqueous solution.[27] Thus, a membrane and a two-compartment electrochemical cell are required in PEC water splitting to protect **NiP** from O$_2$ generated during simultaneous water oxidation at the photoanode (see below).

These results establish mesoTiO$_2$ as an inexpensive, easily-prepared mesoporous cathode material for immobilisation of phosphonate-bearing molecular synthetic catalysts, particularly in terms of the stability of both the material itself and the interaction between the TiO$_2$ and the molecular catalyst, enabling high turnover numbers to be reached and substantial amounts of H$_2$ being generated at a modest overpotential. Our approach thereby complements previous work, where Ni(II) bis(diphosphine) complexes were attached onto electrode surfaces such as silicon[44] and carbon-based materials.[21,45,46] Compared to these previous approaches, TiO$_2$|**NiP** is easier to assemble, requires a less expensive substrate, and can be studied spectroelectrochemically. Furthermore, the transparent nature of TiO$_2$ to visible light and the demonstrated high activity in mild aqueous conditions make TiO$_2$|**NiP** a suitable cathode material for combination with a photoanode to allow for full water splitting, which is difficult to achieve for cathodes operating under the less sustainable conditions used previously.[21,44,46] The use of TiO$_2$ as cathode material in this work is also of interest in the context of current work on its use as a protection layer for photocathode materials such as Cu$_2$O,[7,47] Si[48–50] and CuInS$_2$/CdS,[51] all of which demonstrate photoelectrochemical H$_2$ production in the presence of a Pt catalyst. Employment of phosphonated molecular catalysts such as **NiP** on such TiO$_2$ layers appears as a promising approach to replace expensive noble metals.

Hybrid oxygen-evolving photoanode

Photoanodes composed of molecular hybrid materials developed thus far largely fall into the category of n-type TiO$_2$ sensitised with molecular dyes, including those based on Ru(II),[4,52,53] Zn(II)[54] and organic molecules,[19] and a co-immobilised molecular water oxidation catalyst. Alternatives have been developed utilising visible-light-harvesting semiconductors based on Earth-abundant metal oxides.[23,55–57] Of these, WO$_3$ is notable for good stability under the mildly acidic aqueous conditions required for operation with TiO$_2$|**NiP**,[58] whereas photoanodes made of α-Fe$_2$O$_3$ and BiVO$_4$ are typically studied in alkaline[57,59] and pH neutral conditions,[56,60,61] respectively. It has recently been shown that an immobilised molecular Fe-based catalyst could improve the otherwise poor activity and selectivity[62] for O$_2$ evolution of WO$_3$ in aqueous pH 3 Na$_2$SO$_4$ solution.[23] We therefore assembled a photoanode using WO$_3$,[63] and an Fe(II) catalyst based on a phosphonic acid-modified tris(2-picolyl)amine (TPA) ligand, the unmodified triflate-coordinated analogue of which is known to perform water oxidation homogeneously at low pH in the presence of a chemical oxidant.[12]

Incorporation of a phosphonic acid linker group into the TPA ligand was achieved *via* a multi-step chemical synthesis shown in Scheme 2 (see Experimental section for details). Reductive amination of 4-bromopyridine-2-carboxaldehyde with bis(2-picolyl)amine resulted in the bromine-derivatised TPA compound **1**. The phosphonic acid was introduced first by Pd-catalysed cross coupling[64] to yield the phosphonate ester **2** and subsequently hydrolysed in aqueous HCl to give **TPAp1**·3HCl. The phosphonic acid-modified TPA ligand was coordinated to FeCl$_2$ in methanol in the presence of Et$_3$N to precipitate **FeP** (Scheme 1). **FeP** was synthesised in an overall
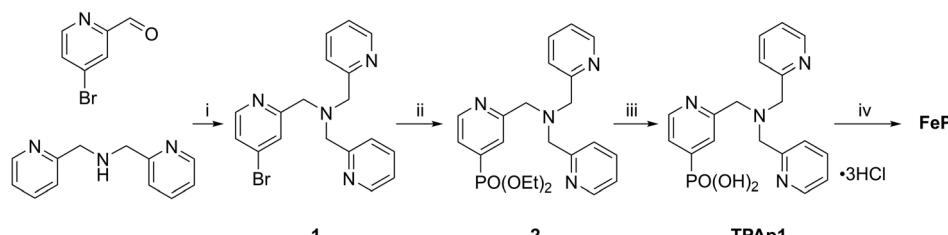
Scheme 2 Synthetic pathway to **FeP**. (i) Na(AcO)$_3$BH (1.2 eq.), CH$_2$Cl$_2$, r.t., 2 d, 66%; (ii) Pd(OAc)$_2$ (4 mol%), 1,1′-bis(diphenylphosphino)ferrocene (5 mol%), Et$_3$N, HPO(OEt)$_2$ (1.1 eq.), 80 °C, 2 d, 67%; (iii) HCl (18% in H$_2$O), reflux, 18 h, 70%; (iv) FeCl$_2$, Et$_3$N, CH$_3$OH, r.t., 47%. Full synthetic and characterisation details can be found in the Experimental section.

yield of 15% from 4-bromo-2-pyridinecarboxaldehyde and characterised by electrospray ionisation mass spectrometry (Fig. S8†), CHN elemental analysis and IR spectroscopy.

The electrochemical response of immobilised **FeP** was first studied on a conducting mesoporous ITO electrode (synthesised as described in the Experimental section). Immobilisation was achieved by submersion in an **FeP** solution (2 mM in methanol) overnight at room temperature, and representative CVs are shown in Fig. S9.† The ITO|**FeP** electrodes displayed a reversible redox wave in pH 3 aqueous solution at $E_{1/2} = 0.7$ V vs. RHE and a linear dependence of the peak current with scan rate supports the immobilisation of **FeP** on the metal oxide electrode surface.

WO$_3$ nanosheet (nanoWO$_3$) electrodes were synthesised hydrothermally onto a WO$_3$ seed layer deposited on FTO as previously described (SEM image shown in Fig. S1b†).[63] Modification of nanoWO$_3$ was achieved by submersion of the electrodes in a methanol solution of **FeP** (2 mM) overnight at room temperature in the dark, and the UV/vis spectrum shows a small

increase in absorbance between 400 and 450 nm (Fig. S10a†), consistent with the presence of **FeP** (Fig. S10b†). Fig. 3a shows an increased photocurrent density (j/mA cm^{-2}) from **FeP**-modified WO$_3$ films in comparison to unmodified films and those treated with FeCl$_2$ and the **TPAp1** ligand was demonstrated by linear sweep voltammetry with chopped illumination ($P = 0.2$ W cm^{-2}, air mass 1.5G). This result suggests an improved photoelectrocatalytic water oxidation by the WO$_3$ film modified with the molecular catalyst, but not the constituent metal salt or ligand in isolation. This result was corroborated by CPE at $E_{appl} = 1.0$ V vs. RHE under illumination, with the charge equivalents and amount of O$_2$ produced shown in Fig. 3b. After 2 h, the WO$_3$|**FeP** was found to produce 3.7 ± 0.4 μmol O$_2$ with 40 ± 4% faradaic efficiency, compared to 1.8 ± 0.3 μmol O$_2$ with 21 ± 2.1% for the unmodified electrode. The low efficiencies can be explained by competing electrolyte oxidation and incomplete oxidation of water known to occur under acidic aqueous conditions,[65] but the increase in selectivity in the presence of the iron(ii) catalyst matched the precedent set previously.[23]

The incident photon-to-current efficiency (IPCE) of WO$_3$|**FeP** was found to vary with the wavelength of incident monochromatic light in accordance with the UV/vis spectrum of WO$_3$ (Fig. S10a†), and made efficient use of the solar spectrum at wavelengths below 450 nm. The IPCE of WO$_3$|**FeP** reached a peak value of 53% at a wavelength of 350 nm, and corresponded to previous reports for catalyst-modified WO$_3$.[66]

Molecule-enabled PEC water splitting

The WO$_3$|**FeP** photoanode displays good water oxidation activity and is compatible with the H$_2$-evolving TiO$_2$|**NiP** cathode in an aqueous pH 3 electrolyte solution. Fig. 4a shows a superposition of the three-electrode linear sweep voltammograms of the individual electrodes. The voltammograms of the individual electrodes imply that if the TiO$_2$|**NiP** cathode and WO$_3$|**FeP** photoanode are combined in a two-electrode PEC configuration, the onset of photocurrent should be at an applied voltage of approximately 0.6 V. This is lower than the thermodynamic potential requirement for water splitting (1.23 V) and the proposed device should have capacity for solar energy storage in the fuel H$_2$.

We therefore assembled a two-electrode PEC cell, with WO$_3$|**FeP** as the photoanode under periodic simulated solar light
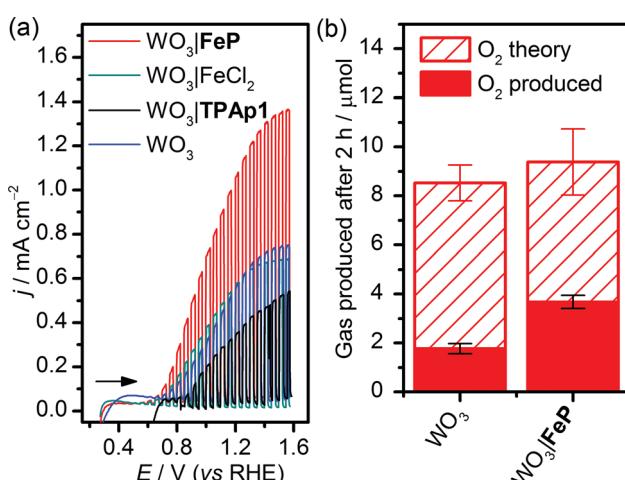

Fig. 3 (a) LSVs under chopped illumination (AM1.5G, 0.2 W cm^{-2}) of WO$_3$ (blue line), WO$_3$|**FeP** (red line), WO$_3$|FeCl$_2$ (green line) and WO$_3$|**TPAp1** (black line) at $\nu = 5$ mV s^{-1}. (b) Amount of O$_2$ generated after two h PEC water oxidation by nanoWO$_3$ with and without **FeP** under solar illumination at $E_{appl} = 1.0$ V vs. RHE. The theoretical amount of O$_2$ was calculated based on 100% faradaic yield and the experimentally measured O$_2$ was quantified by a fluorescence probe. Conditions: a Ag/AgCl reference electrode and a Pt mesh counter electrode in aqueous Na$_2$SO$_4$ (0.1 M) solution at pH 3, N$_2$ atmosphere and room temperature.
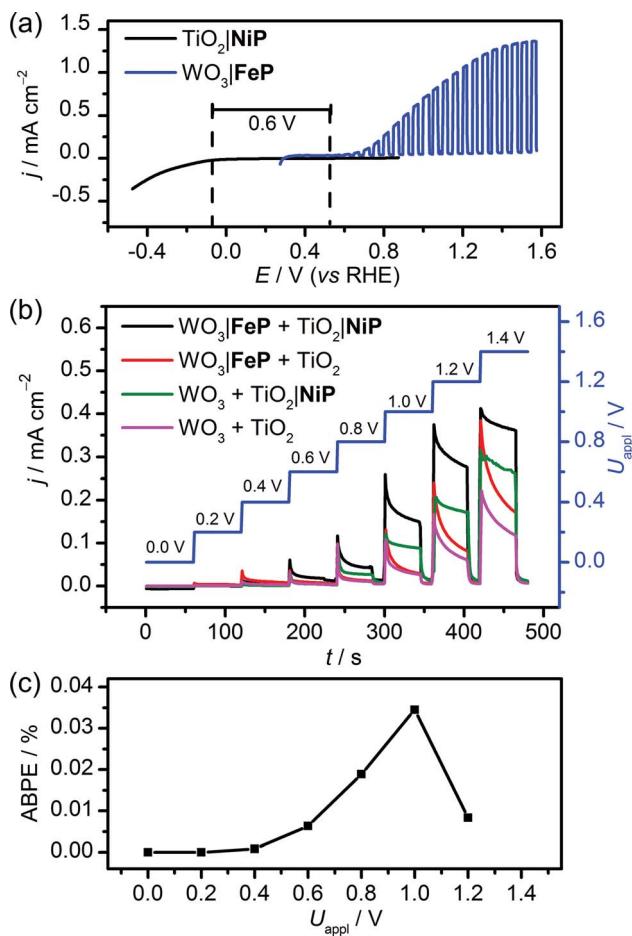
Fig. 4 Comparison between (a) superimposed three-electrode LSVs with TiO$_2$|NiP and WO$_3$|FeP (ν = 5 mV s^{-1}) and (b) two-electrode, stepped-potential PEC water splitting with TiO$_2$|NiP directly wired to WO$_3$|FeP (control experiments in the absence of one or both molecular catalysts are also shown). (c) Applied bias photon-to-current efficiency (ABPE) for the cell comprising both catalyst-modified electrodes. Conditions: aqueous Na$_2$SO$_4$ (0.1 M) electrolyte solution at pH 3 and room temperature with solar light irradiation (100 mW cm^{-2} AM1.5G) using a TiO$_2$|NiP cathode (geometrical surface area: 1.0 cm^2, shielded from irradiation) and a WO$_3$|FeP photoanode (0.5 cm^2).

irradiation and TiO$_2$|**NiP** (shielded from the illumination to avoid UV band gap excitation of TiO$_2$) as the cathode, with the electrodes separated by a proton-permeable Nafion membrane to prevent gas diffusion between the cathodic and anodic compartments (Scheme 1). As predicted from the voltammetric response of the individual electrodes, a notable photocurrent was observed at U_{appl} = 0.6 V in the two-electrode configuration linear sweep voltammogram shown in Fig. 4b. This demonstrates energy storage across the electrodes without the need for a precious-metal containing component (catalyst and electrode material). In the absence of **NiP**, the photocurrent decayed quickly within each 45 s illumination period, due to initial reductive charging of the TiO$_2$ (Fig. 4b). The applied bias (U_{appl}) photon-to-current conversion efficiency (ABPE, Fig. 4c) for the PEC cell was calculated with eqn (1), with the photocurrent density (j/mA cm^{-2}) taken after 45 s illumination at each U_{appl}

under full simulated solar spectrum irradiation with a light intensity (P) of 100 mW cm^{-2}.

$$\text{ABPE } (\%) = \left[\frac{(j/\text{mA cm}^{-2}) \times (1.23 - (U_{appl}/V))}{P/\text{mW cm}^{-2}} \right] \times 100 \tag{1}$$

The ABPE was found to have a maximum at U_{appl} = 1.0 V with an ABPE = 0.035%. The low value for ABPE is due to incomplete use of the solar spectrum by WO$_3$ shown in Fig. S10a† (note that the full simulated solar spectrum, not monochromatic light, was used to calculate the ABPE) and a relatively large applied bias required to achieve a significant photocurrent. Nevertheless, this efficiency is comparable to the only other efficiency reported for a fully molecular solar PEC water splitting cell with a solar-to-hydrogen (STH) efficiency of 0.05%, which required the use of precious metals. However it should be noted that STH accounts for the faradaic efficiency of H$_2$ production, unlike the APBE presented here.[19]

It was essential to perform extended PEC water splitting under simulated solar light illumination for an in-depth assessment of the efficacy of the molecular catalysts. An electrochemical bias of 1.1 V, less than the thermodynamic potential for water splitting, was applied, and the generated charge, amounts of O$_2$ and H$_2$ are summarised in Table 1 and Fig. 5. After 1 h, 0.61 ± 0.06 µmol of O$_2$ were detected by a fluorescence sensor (Fig. S11†) and 1.04 ± 0.29 µmol of H$_2$ were analysed by gas chromatography with faradaic efficiencies of 61 ± 5% and 53 ± 17%, respectively. The O$_2$-to-H$_2$ ratio was close to the expected one-to-two ratio for full water splitting. Consistent with the three-electrode experiments was the observation that in the absence of **FeP**, no or only traces of oxygen were detected, again demonstrating the increased selectivity offered by the molecular **FeP** catalyst in these conditions. The lower faradaic efficiency for H$_2$ evolution compared to the three-electrode CPE (Table 1) may be due to initial competitive reduction of O$_2$ or other contaminants trapped within the mesoporous TiO$_2$ electrode in the early stages of electrolysis, as has been observed previously for other nanostructured electrodes.[67] In agreement, we observed a faradaic efficiency of 58 ± 13% for H$_2$ generation with TiO$_2$|**NiP** after 1 h CPE in the experiments shown in Fig. 2a.

Without **NiP**, low photocurrents and consequently lower gaseous products were detected, showing that the molecular catalyst is required to perform proton reduction at a sufficiently low overpotential to be coupled to water oxidation in this system. We also performed two-electrode PEC water splitting of the molecular catalyst-modified electrodes at zero-energy storage (U_{appl} = 1.23 V $vs.$ RHE) for 1 h, with the results summarised in Table 1. We observed a higher H$_2$ (2.3 ± 0.4 µmol, 83 ± 16% faradaic yield) and O$_2$ (0.82 ± 0.10 µmol, 60 ± 20% faradaic yield) evolution activity than at U_{appl} = 1.1 V. These results demonstrate that the molecular catalysts based on Earth-abundant transition metals are also capable of driving water splitting at a higher rate if better electrode materials become available. A tandem PEC device with a suitable photocathode modified with **NiP** wired to WO$_3$|**FeP** would

Table 1 Key performance parameters of the electrodes employed in this work[a]

Three-electrode configuration[b]

Description	E_{appl}/V vs. RHE	Time/h	$n(H_2)$/µmol	Faradaic yield (%)	$n(O_2)$/µmol	Faradaic yield (%)
TiO$_2$|**NiP**	−0.25	8	9.3 ± 2.1	88 ± 17		
TiO$_2$	−0.25	8	0.07 ± 0.03	5.6 ± 1.7		
TiO$_2$|**NiP**[c]	−0.25	4	0.58 ± 0.24	7.4 ± 4.5		
WO$_3$|**FeP**	1.0	2			3.7 ± 0.4	40 ± 4
WO$_3$	1.0	2			1.8 ± 0.3	21 ± 2.1

Two-electrode PEC water splitting

Description	U_{appl}/V	Time/h	$n(H_2)$/µmol	Faradaic yield (%)	$n(O_2)$/µmol	Faradaic yield (%)
TiO$_2$|**NiP** + WO$_3$|**FeP**	1.1	1	1.04 ± 0.29	53 ± 17	0.61 ± 0.06	61 ± 6
TiO$_2$|**NiP** + WO$_3$	1.1	1	0.51 ± 0.19	47 ± 14	0.09 ± 0.02	18 ± 6
TiO$_2$ + WO$_3$|**FeP**	1.1	1	0.21 ± 0.1	38 ± 13	0.08 ± 0.08	26 ± 26
TiO$_2$ + WO$_3$	1.1	1	0.41 ± 0.26	60 ± 18	—[d]	—
TiO$_2$|**NiP** + WO$_3$|**FeP**	1.23	1	2.3 ± 0.4	83 ± 16	0.82 ± 0.10	60 ± 20

[a] Conditions: aqueous Na$_2$SO$_4$ (0.1 M) solution at pH 3 in a two compartment (photo)electrochemical cell at room temperature. Unless otherwise stated, the cell purged with N$_2$ before each experiment and CH$_4$ (2%) was present as internal standard for H$_2$ quantification by GC. The WO$_3$ photoanode was illuminated with solar light (AM1.5G) at 0.2 W cm^{-2} in the three-electrode experiments and 0.1 W cm^{-2} in two-electrode PEC water splitting. The TiO$_2$ cathode was shielded from illumination. [b] A Pt counter electrode and a Ag/AgCl reference electrode were employed. [c] Performed under air with CH$_4$ as external standard. [d] Below the limit of detection.
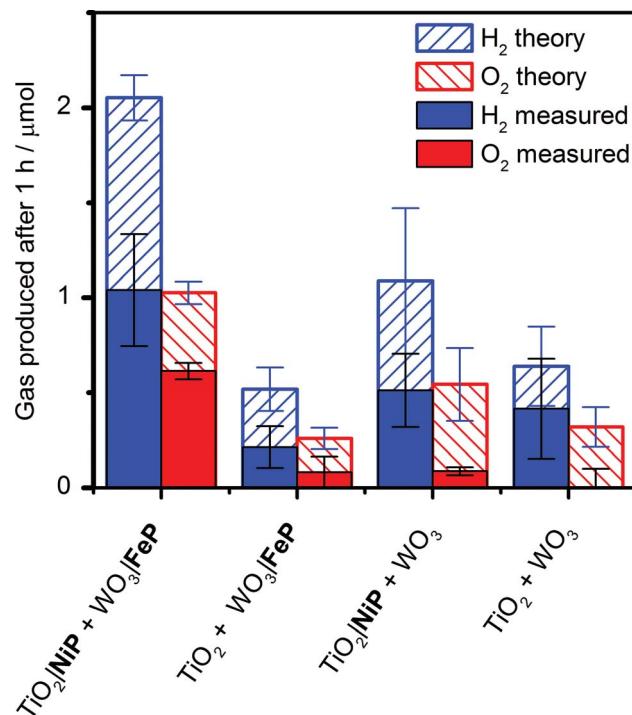
Fig. 5 Summary of theoretical and practical H$_2$ and O$_2$ production by two-electrode PEC water splitting with TiO$_2$\|**NiP** cathode (geometrical surface area: 1.0 cm^2, shielded from irradiation) wired to WO$_3$\|**FeP** photoanode (0.5 cm^2) and control experiments without one or both molecular catalysts. The theoretical amount of gaseous products were calculated based on 100% faradaic yield. Conditions: aqueous Na$_2$SO$_4$ (0.1 M) electrolyte solution at pH 3, N$_2$ atmosphere and room temperature with an applied bias (U_{appl}) = 1.1 V for 1 h and solar light illumination (100 mW cm^{-2}, AM1.5G).
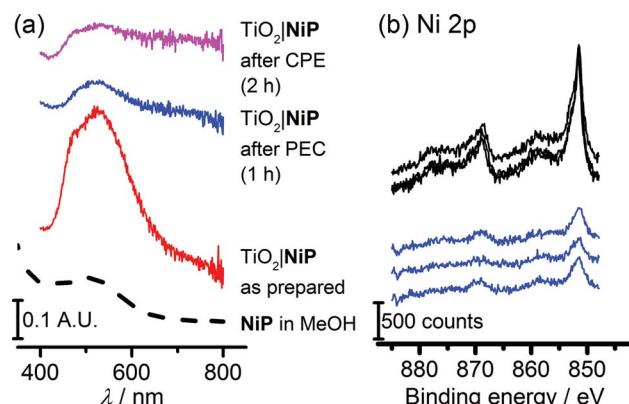
Fig. 6 (a) Diffuse-reflectance UV-vis absorption spectra of **NiP**-modified TiO$_2$ electrodes as prepared (red line), after 1 h PEC electrolysis at U_{appl} = 1.1 V, and after 2 h CPE at E_{appl} = −0.33 V vs. RHE, with a MeOH solution UV-vis spectrum as a reference (dashed line). (b) X-ray photoelectron spectra in the Ni 2p region of TiO$_2$\|**NiP** and electrodes before (black line) and after (blue line) 1 h PEC electrolysis at U_{appl} = 1.1 V with WO$_3$\|**FeP**.

dramatically reduce the applied bias and result in higher photocurrents and ABPE in the future.[7,68]

Molecular integrity of catalysts in PEC water splitting

The study of molecular catalysts under strongly reductive and oxidative conditions requires an assessment of their integrity during catalysis.[69] For instance, Fe-based catalysts related to **FeP** are known to remain molecular during water oxidation in homogeneous aqueous acidic conditions, but to oxidise to catalytically-active iron oxide nanoparticles under basic conditions.[70] Although Ni-based molecular compounds have also

been reported to decompose to catalytically-active Ni-containing nanoparticles under reductive conditions,[71] this has not been observed for **NiP** in solution or in suspensions with semiconducting nanoparticles.[14,20,26,27] Fig. 6a shows diffuse reflectance UV-vis spectra of the **NiP**-modified mesoTiO$_2$ electrode. Before electrolysis, the electrodes were purple in colour and showed a broad band at λ_{max} = 520 nm in the UV-vis spectrum of **NiP**. The purple colour with the band at λ_{max} = 520 nm were qualitatively retained following three-electrode CPE for 2 h and two-electrode solar water electrolysis coupled to WO$_3$|**FeP** for 1 h, indicating that molecular **NiP** remained on mesoTiO$_2$.

X-ray photoelectron spectroscopy (XPS) on both modified electrodes before and after running 1 h PEC water splitting at an applied bias of 1.1 V were performed to analyse the possible formation of metal-containing deposits. The Ni(2p) or Fe(2p) : N(1s) : P(2p) ratios, of approximately 1 : 4 : 8 for TiO$_2$|**NiP** and 1 : 4 : 1 for WO$_3$|**FeP**, before two-electrode PEC water splitting were as expected (Scheme 1 and Table S1†). In agreement with previous work, for WO$_3$|**FeP**, no Fe peak was observed after PEC water splitting (Fig. S12†), suggesting that no iron-based deposit was formed on the electrode. Instead it is postulated that the iron(II) catalyst slowly desorbs from the electrode surface during photoelectrocatalysis,[23] possibly due to the presence of only one phosphonate anchor group on **FeP**. Therefore, the limiting electrode in this PEC water splitting cell is the **FeP**-modified WO$_3$ photoanode.

Peaks corresponding to Ni(2p), N(1s) and P(2p) were retained after catalysis (Fig. 6b and S13†), and remained in the same ratio before and after PEC water splitting for TiO$_2$|**NiP**. Fig. 6b and the peak positions in Table S2† demonstrate that the Ni(2p) peak binding energies at 851.5 eV and 869 eV remain unchanged during PEC water splitting, and no new peaks were observed that could correspond to a new Ni-based species. The combination of the unchanged elemental ratios, unaltered peak positions in XPS and diffuse reflectance UV-vis data provides strong evidence that the molecular structure of **NiP** remains intact during electrolysis immobilised on mesoTiO$_2$ electrodes. This result emphasises the suitability of molecular electro-catalyst design even when working on heterogeneous catalytic systems.

Conclusions

We have presented a hybrid proton reduction cathode based on a phosphonated Ni(II) bis(diphosphine) molecular catalyst and mesostructured TiO$_2$, which is normally considered an insulator in the absence of UV irradiation and therefore of limited use in electrocatalysis. We observed, from complementary cyclic voltammetry and spectroelectrochemistry, that at mildly reducing potentials electrons are transferred first to the CB of TiO$_2$, and then to **NiP** for proton reduction catalysis. During long term controlled-potential electrolysis, sustained H$_2$ production was observed at an applied potential of E_{appl} = −0.25 V *vs.* RHE, with a **NiP**-based turnover number of 600 achieved after 8 hours. Characterisation and quantification of the catalyst after electrolysis revealed not only that the molecular structure was intact, but also 75% of the **NiP** initially

present remained on the electrode surface. The modified TiO$_2$ performed considerably better than an analogous mesoporous ITO electrode, which underwent degradation under reducing conditions. Therefore, the TiO$_2$|**NiP** cathode exhibited excellent stability in terms of the material itself, the molecular structure of the catalyst, and the attachment between the two in mildly acidic aqueous conditions. These results establish TiO$_2$|**NiP** as not only an effective H$_2$ evolving electrode in its own right, but also suggest potential as a catalytically-active protection layer for photocathodes due to its ease of preparation, transparency to visible light, stability and high activity at a modest overpotential.

We have demonstrated the utility of this cathode by constructing a precious-metal-free two-compartment PEC cell for full water splitting with molecular catalysts crucial to the performance of both the photoanode and the cathode for the first time. Under solar illumination and an applied bias of U_{appl} = 1.1 V, below the thermodynamic potential for water splitting, an approximately 2 : 1 ratio of H$_2$: O$_2$ was only obtained in the presence of **FeP** and **NiP**. Essential to this achievement was the development of hybrid electrodes operable under the same mild conditions. We have also presented a number of experiments showing consistent evidence that the molecular structure of **NiP** remained intact after the photoelectrolysis experiments, a result which emphasises the importance in molecular catalyst design in the development of molecule/material hybrids. These results demonstrate that if mild conditions are used, molecular catalysts can remain stable and effective under catalytic conditions. The immobilisation approach and characterisation techniques reported here provide a promising framework for the future systematic study of the activity and stability of a variety of molecular catalysts in environmentally-benign aqueous solution.

Experimental section

Materials and methods

All starting materials were obtained from commercial sources and used without further purification, unless otherwise stated. ITO nanopowder (<50 nm particle size) was obtained from Sigma-Aldrich and P25 TiO$_2$ (8 : 2 anatase : rutile, 20 nm average particle size) from Evonik Industries. **NiP**[20] and 4-bromo-2-pyridinecarboxaldehyde[72] were synthesised following literature procedures. Dry solvents were dried and distilled under N$_2$ prior to use, or in the case of methanol purchased as dry solvent and stored over molecular sieves. Solvent mixtures are reported as vol : vol ratios. Standard Schlenk line techniques were used where required. ^{1}H, ^{13}C and ^{31}P NMR measurements were performed on a Bruker DPX400 spectrometer. Mass spectrometry measurements were performed on a Waters Micromass Quattro LS ESI or ThermoScientific Orbitrap Classic instrument (calculated and experimental isotope patterns were compared). SEM was performed on a FEI Phillips XL30 field emission gun SEM instrument. XPS was performed by the Nexus facility at the University of Newcastle on a K-Alpha (Thermo Scientific, East Grinstead, UK) spectrometer utilising a monochromatic Al-Kα X-ray source (1486.6 eV, 400 μm spot size, 36 W). Survey spectra were collected with a pass energy of

200 eV and 3 sweeps, while high resolution spectra were collected at a pass energy of 40 eV with 10 sweeps. Elemental analysis was carried out by the University of Cambridge Microanalysis Service using a Perkin-Elmer 240 Elemental Analyser. UV-vis absorption spectroscopy was performed using a Varian Cary 50 spectrophotometer. Where stated, a diffuse reflectance accessory for the spectrophotometer was used, with a Spectralon reference as a background. UV-vis spectra (reflectance mode) of WO_3 were recorded on an Edinburgh Instruments FS5 spectrofluorometer equipped with an integrating sphere by running a synchronous scan ($\lambda_{ex} = \lambda_{em}$) and subtracting a scan of the sphere background. ATR-FTIR measurements were performed on a Nicolet iS50 FTIR spectrometer.

Synthesis and characterisation

Bis(2-methylpyridyl)(4-bromo-2-methylpyridyl)amine (1). This compound was synthesised by adaptation of a literature procedure for tris(2-pyridylmethyl)amine.[72] In a pre-dried Schlenk flask, sodium tri(acetoxy)borohydride (1.7 g, 6.6 mmol) was dried *in vacuo*. Dry CH_2Cl_2 (50 mL) was added, followed by 4-bromo-2-pyridinecarboxaldehyde (1.0 g, 5.6 mmol) and di-(2-picolyl)-amine (1.0 mL, 4.7 mmol). The mixture was degassed by three freeze–pump–thaw cycles, purged with N_2 and stirred under N_2 at room temperature for 2 d. Saturated aqueous $NaHCO_3$ (20 mL) was added, and the biphasic mixture stirred for 1 h. The crude product was extracted in CH_2Cl_2 (3 × 25 mL), washed with brine (20 mL), dried over $MgSO_4$ and the solvent removed *in vacuo*. Purification was achieved by flash column chromatography on silica (pre-deactivated with Et_3N), eluting in CH_2Cl_2 : Et_3N (98 : 2) to yield **1** as a pale yellow oil (yield: 1.1 g, 66%). HR-MS calc. for $[C_{18}H_{18}BrN_4]^+$: 369.0709, found: 369.0724 (100% peak); ^{1}H-NMR (400 MHz, $CDCl_3$) δ/ppm: 8.58 (d, $J = 4.1$ Hz, 2H), 8.36 (d, $J = 5.3$ Hz, 1H), 7.80 (d, $J = 1.5$ Hz, 1H), 7.70 (td, $J = 7.7$, 1.6 Hz, 2H), 7.56 (d, $J = 7.6$ Hz, 2H), 7.34 (dd, $J = 5.3$, 1.8 Hz, 1H), 7.18 (dd, $J = 6.6$, 5.1 Hz, 2H), 3.93 (s, 4H, CH_2), 3.91 (s, 2H, CH_2); ^{13}C NMR (101 MHz, $CDCl_3$) δ/ppm 149.82, 148.46, 137.52, 136.93, 133.62, 126.67, 125.82, 123.75, 122.74, 120.88, 60.40, 59.33.

Bis(2-methylpyridyl)(4-(diethylphosphonate)-2-methylpyridyl)-amine (2). In a pre-dried Schlenk flask with a Teflon screw-cap, palladium(II) acetate (25 mg, 0.11 mmol) and 1,1′-bis(diphenylphosphino)ferrocene (dppf, 75 mg, 0.14 mmol) were dried *in vacuo*. In a separate pre-dried flask, **1** (1.0 g, 2.7 mmol) was added and the flask evacuated and purged with N_2 three times. The compound was dissolved in dry acetonitrile (6 mL) and added to the reaction flask under N_2. Diethyl phosphite (0.40 mL, 2.9 mmol) and Et_3N (1 mL) were added and the mixture was degassed by three freeze–pump–thaw cycles. The flask was heated to 70 °C under N_2, sealed, and stirred at 70 °C for 2 d. The reaction mixture was cooled, the solvent removed *in vacuo*, and the product purified by flash column chromatography on silica (pre-deactivated with Et_3N), eluting with CH_2Cl_2 : Et_3N : CH_3OH (97.5 : 2 : 0.5) to yield **2** as a yellow oil that discoloured quickly and solidified on standing (yield: 0.78 g, 67%). HR-MS calc. for $[C_{22}H_{28}N_4O_3P]^+$: 427.1894, found 427.1875 (100% peak); ^{1}H-NMR (400 MHz, $CDCl_3$) δ/ppm: 8.68 (t, $J = 5.0$ Hz, 1H), 8.53 (d, $J = 4.0$ Hz, 2H), 7.96 (d, $J = 14.1$ Hz, 1H), 7.67 (td, $J = 7.5$, 1.0 Hz, 2H),

7.58 (d, $J = 8.0$ Hz, 2H), 7.50 (dd, $J = 13.1$, 4.0 Hz, 1H), 7.15 (dd, $J = 6.3$, 5.3 Hz, 2H), 4.06–4.24 (m, 4H), 3.97 (s, 2H), 3.90 (s, 4H), 1.34 (t, $J = 7.0$ Hz, 6H); ^{13}C (101 MHz, $CDCl_3$) δ/ppm: 160.74 (d, $J = 12.0$ Hz), 159.45 (s), 149.78 (d, $J = 12.8$ Hz), 149.48 (s), 138.16 (d, $J = 187.7$ Hz), 136.86 (s), 124.92 (d, $J = 8.8$ Hz), 123.83 (d, $J = 8.8$ Hz), 123.39 (s), 122.47 (s), 63.07 (d, $J = 5.6$ Hz), 60.60 (s), 60.37 (s), 16.72 (d, $J = 6.4$ Hz) ^{31}P-NMR (162 MHz, $CDCl_3$) δ/ppm: −16.31; IR $\nu = 1250$ cm^{-1} (P=O).

Bis(2-methylpyridyl)(4-phosphonic acid-2-methylpyridyl)amine hydrochloride (TPAp1·3HCl). Compound **2** (0.5 g, 1.2 mmol) was dissolved in 18% aqueous HCl (4 mL) and refluxed for 18 h. The reaction mixture was cooled to r.t. and the solvent was removed *in vacuo* and the brown oily crude dissolved in CH_3OH. Precipitation with EtOAc followed by filtration and washing with EtOAc yielded **TPAp1·3HCl** as a hygroscopic off-white powder (yield: 0.40 g, 70%). MS calc. for $[C_{18}H_{20}N_4O_3P]^+$: 371.12 (100.0%), found: 371.0 (100%); ^{1}H-NMR (400 MHz, D_2O) δ/ppm: 8.65 (d, $J = 5.6$ Hz, 2H), 8.60 (br. s., 1H), 8.42 (t, $J = 7.9$ Hz, 2H), 7.99 (m, 3H), 7.86 (m, 3H), 4.35 (s, 4H), 4.27 (br. s., 2H, CH_2); ^{13}C-NMR (101 MHz, D_2O) δ/ppm: 151.42 (d, $J = 12.1$ Hz), 151.00 (s), 147.52 (s), 144.34 (d, $J = 321.6$ Hz), 142.09 (d, $J = 12.1$ Hz), 141.91 (s), 127.85 (d, $J = 9.5$ Hz), 127.53 (s), 127.16 (d, $J = 8.7$ Hz), 126.78 (s), 56.37 (s); ^{31}P-NMR (162 MHz, D_2O) δ/ppm: −4.36; IR $\nu = 1170$ cm^{-1} (P=O); EA calc. for $C_{18}H_{26}Cl_3N_4O_5P$ (**TPAp1·3HCl·2H$_2$O**) C, 41.92; H, 5.08; N, 10.86; P, 6.01, found C 42.51, H 5.01, N 10.42, P 5.81.

[FeCl(MeO)(TPAp1)] (FeP). In a pre-dried Schlenk flask, **TPAp1·3HCl** (40 mg, 0.084 mmol) was dissolved in dry CH_3OH under N_2. Dry Et_3N (50 μL, 0.33 mmol) was added, and the solution stirred under for 30 min. This solution was added to a degassed solution of anhydrous $FeCl_2$ (11 mg, 0.084 mmol) in CH_3OH (2 mL). The solution was freeze–pump–thaw degassed three times, and stirred under N_2 for 2 h. The solvents were removed *in vacuo*, CH_3CN (4 mL) was added, and the suspension stirred under N_2 for 12 h to dissolve the Et_3NHCl. The suspension was filtered off and the precipitate dried *in vacuo* to give **FeP** as a red powder (yield: 20 mg, 47%). MS calc. for $[Fe(TPAp1)Cl]^+$: m/z: 461.022 (100.0%), found 460.97 (100%); EA calc. for $C_{19}H_{23}ClFeN_4O_3P$ [**TPAp1FeCl(OMe)**] C, 46.32; H, 4.50; N, 11.37; found C, 46.02; H, 4.85 N, 11.60; IR $\nu = 1170$ cm^{-1} (P=O).

Preparation of nanostructured metal oxide electrodes

Prior to preparation of mesoporous electrodes, glass slides coated with indium-doped tin oxide (ITO) for mesoITO or fluorine-doped tin oxide (FTO) for mesoTiO$_2$ of dimensions 3.0 cm × 1.0 cm were cleaned by heating at 70 °C in a 5 : 1 : 1 solution of H_2O : H_2O_2 (30% aq.) : NH_4OH (conc. aq.) for 30 min, followed by rinsing with H_2O and drying at 180 °C for 1 h. Suspensions of ITO (20% by weight of ITO in a 5 M acetic acid solution in ethanol) and TiO_2 nanoparticles (100 mg TiO_2 and 50 mg poly-(ethylene glycol) in approximately 1 mL ethanol) were applied to the transparent conducting oxide-coated glass slides using the doctor blading method using a Scotch tape mask with aperture dimensions of either a 6 mm diameter circle (for cyclic voltammetry) or a 0.7 cm × 1.5 cm rectangle (for (photo)electrolysis). The slides were then annealed at 450 °C for 0.5 h (mesoTiO$_2$) or at 400 °C for 1 h (mesoITO).

The mesoTiO$_2$ and mesoITO electrodes were cleaned and dried with ammonia/hydrogen peroxide (see above) and/or using a BioForce UV/ozone cleaner. Immobilisation was achieved by submersion of the electrodes in a 0.5 mM solution of **NiP** in methanol for 18 h. The coverage of **NiP** was quantified by submersion of the modified electrodes in a NaOH$_{(aq)}$ solution (0.1 M) for 30 min, followed by UV-vis spectroscopy of the resultant solution and comparison with calibration data at $\lambda = 257$ and 300 nm.

WO$_3$ electrodes were prepared as previously described by hydrothermal synthesis,[63] and were characterised by SEM to reveal a nanosheet morphology (Fig. S1b†). Electrode areas were masked to 1.5 cm^2 for three-electrode measurements and 0.5 cm^2 for two-electrode measurements.

Electrochemical methods

All electrochemical measurements were performed on Ivium Technologies CompactStat or IviumStat, or PalmSens EmStat or MultiEmStat^{3+} potentiostats. All electrochemical measurements were performed in a Na$_2$SO$_4$ (0.1 M) aqueous solution, adjusted to the desired pH by titration with H$_2$SO$_4$ at room temperature and purged with N$_2$ unless otherwise stated. Electrochemical experiments on the individual TiO$_2$|NiP cathode or WO$_3$|FeP photoanode were performed in a three-electrode configuration with a Pt counter electrode and a Ag/AgCl/KCl$_{(sat)}$ reference electrode, whereas full water splitting CPE experiments were performed in a two-electrode setup with TiO$_2$|NiP directly (shielded from illumination) connected to WO$_3$|FeP in a two-compartment airtight cell. Irradiation was provided through a quartz illumination window and the cathode was separated from the anode by a Nafion membrane. Simulated solar irradiation was provided by a Newport solar light simulator with an AM1.5G filter and a water IR filter. TiO$_2$ was shielded from light to avoid UV band gap excitation. Light intensity was measured using an International Light Technologies 1400 photometer. IPCE measurements were performed using monochromatic light provided by a LOT 300 W Xe lamp equipped with a MSH300 monochromator (FWHM = 5 nm). IPCE was calculated using eqn (2).

$$\text{IPCE (\%)} = \frac{I_{el}}{I_{ph}} \times 100 = \frac{j \times 10^{-2}}{\dfrac{F}{\dfrac{W \times \lambda \times 10^{-9}}{N_A \times h \times c}}} \times 100 \qquad (2)$$

where I_{el} is the electron flux of the external circuit (mol m^{-2} s^{-1}), I_{ph} is the incident photon flux (mol m^{-2} s^{-1}), j is the measured photocurrent density (μA cm^{-2}), F is the Faraday constant (96 484 A s mol^{-1}), λ is the wavelength of light (nm), W is the incident power of the monochromated light (W m^{-2}), N_A is Avogadro's number (6.022 $\times$ 10^{23} mol^{-1}), h is Planck's constant (6.626 $\times$ 10^{-34} J s) and c is the speed of light (2.998 $\times$ 10^8 m s^{-1}).

Resistance between electrodes in the two compartments was found to be <100 Ω by electrochemical impedance spectroscopy and the reported voltages are not corrected for cell resistance. The experiments were performed at room temperature, and the cell was purged with an inert gas before each experiment. All reduction potentials from the three-electrode experiments are reported against RHE using eqn (3).

$$E_{RHE}/V = E_{Ag/AgCl}/V + 0.197 + 0.059 \times \text{pH} \qquad (3)$$

Spectroelectrochemical measurements were performed in a borosilicate glass one-compartment electrochemical cell purged with N$_2$ in the beampath of a Varian Cary 50 spectrophotometer.

Quantification of gaseous products

Oxygen detection was performed using an Ocean Optics NeoFox phase fluorimeter equipped with a FOSPOR probe calibrated in the 0–3% O$_2$ regime using a mass-flow controller. The chamber containing the oxygen probe (in the headspace, inserted through a rubber septum) was degassed by purging the solution with N$_2$ for 30 min. Background O$_2$ was then recorded for 30 min, before commencement of the photoelectrolysis experiment. Finally, a further 30 min background was run after ceasing illumination and the background levels of O$_2$ were subtracted. The total amount of O$_2$ produced was obtained using the ideal gas law for O$_2$ in the headspace, and Henry's law for dissolved O$_2$.

For H$_2$ quantification, the cell was purged with N$_2$/CH$_4$ (2%) for 10 min prior electrochemical experiments. The H$_2$ produced was quantified by an Agilent 7890A gas chromatograph, with CH$_4$ as an internal standard. For experiments performed under air, CH$_4$ was used as an external standard. Gas detection experiments were repeated 3 times and values given as an average of the three $\pm$ standard deviation.

Acknowledgements

References

1 F. Lakadamyali, A. Reynal, M. Kato, J. R. Durrant and E. Reisner, *Chem.–Eur. J.*, 2012, **18**, 15464–15475.

2 M. Kirch, J.-M. Lehn and J.-P. Sauvage, *Helv. Chim. Acta*, 1979, **62**, 1345–1384.

3 D. V. Esposito and J. G. Chen, *Energy Environ. Sci.*, 2011, **4**, 3900–3912.

4 Y. Gao, X. Ding, J. Liu, L. Wang, Z. Lu, L. Li and L. Sun, *J. Am. Chem. Soc.*, 2013, **135**, 4219–4222.

5 L. Alibabaei, M. K. Brennaman, M. R. Norris, B. Kalanyan, W. Song, M. D. Losego, J. J. Concepcion, R. A. Binstead,

G. N. Parsons and T. J. Meyer, *Proc. Natl. Acad. Sci. U. S. A.*, 2013, **110**, 20008–20013.

6 S. Y. Reece, J. A. Hamel, K. Sung, T. D. Jarvi, A. J. Esswein, J. J. H. Pijpers and D. G. Nocera, *Science*, 2011, **334**, 645–648.

7 C.-Y. Lin, Y.-H. Lai, D. Mersch and E. Reisner, *Chem. Sci.*, 2012, **3**, 3482–3487.

8 D. Mersch, C.-Y. Lee, J. Z. Zhang, K. Brinkert, J. C. Fontecilla-Camps, A. W. Rutherford and E. Reisner, *J. Am. Chem. Soc.*, 2015, **137**, 8541–8549.

9 E. S. Andreiadis, M. Chavarot-Kerlidou, M. Fontecave and V. Artero, *Photochem. Photobiol.*, 2011, **87**, 946–964.

10 Z. Yu, F. Li and L. Sun, *Energy Environ. Sci.*, 2015, **8**, 760–775.

11 J. Willkomm, N. M. Muresan and E. Reisner, *Chem. Sci.*, 2015, **6**, 2727–2736.

12 J. L. Fillol, Z. Codolà, I. Garcia-Bosch, L. Gómez, J. J. Pla and M. Costas, *Nat. Chem.*, 2011, **3**, 807–813.

13 S. Roy, M. Bacchi, G. Berggren and V. Artero, *ChemSusChem*, 2015, **8**, 3632–3638.

14 B. C. M. Martindale, G. A. M. Hutton, C. A. Caputo and E. Reisner, *J. Am. Chem. Soc.*, 2015, **137**, 6018–6025.

15 W. M. Singh, D. Pegram, H. Duan, D. Kalita, P. Simone, G. L. Emmert and X. Zhao, *Angew. Chem., Int. Ed.*, 2012, **51**, 1653–1656.

16 P. Farràs, C. Di Giovanni, J. N. Clifford, E. Palomares and A. Llobet, *Coord. Chem. Rev.*, 2015, **304–305**, 202–208.

17 A. Reynal, J. Willkomm, N. M. Muresan, F. Lakadamyali, M. Planells, E. Reisner and J. R. Durrant, *Chem. Commun.*, 2014, **50**, 12768–12771.

18 K. Fan, F. Li, L. Wang, Q. Daniel, E. Gabrielsson and L. Sun, *Phys. Chem. Chem. Phys.*, 2014, **16**, 25234–25240.

19 F. Li, K. Fan, B. Xu, E. Gabrielsson, Q. Daniel, L. Li and L. Sun, *J. Am. Chem. Soc.*, 2015, **137**, 9153–9159.

20 M. A. Gross, A. Reynal, J. R. Durrant and E. Reisner, *J. Am. Chem. Soc.*, 2014, **136**, 356–366.

21 A. Le Goff, V. Artero, B. Jousselme, P. D. Tran, N. Guillet, R. Métayé, A. Fihri, S. Palacin and M. Fontecave, *Science*, 2009, **326**, 1384–1387.

22 M. L. Helm, M. P. Stewart, R. M. Bullock, M. Rakowski DuBois and D. L. DuBois, *Science*, 2011, **333**, 863–866.

23 B. M. Klepser and B. M. Bartlett, *J. Am. Chem. Soc.*, 2014, **136**, 1694–1697.

24 A. D. Wilson, R. H. Newell, M. J. McNevin, J. T. Muckerman, M. Rakowski DuBois and D. L. DuBois, *J. Am. Chem. Soc.*, 2006, **128**, 358–366.

25 A. Dutta, S. Lense, J. Hou, M. H. Engelhard, J. A. S. Roberts and W. J. Shaw, *J. Am. Chem. Soc.*, 2013, **135**, 18490–18496.

26 C. A. Caputo, M. A. Gross, V. W. Lau, C. Cavazza, B. V. Lotsch and E. Reisner, *Angew. Chem., Int. Ed.*, 2014, **53**, 11538–11542.

27 D. W. Wakerley, M. A. Gross and E. Reisner, *Chem. Commun.*, 2014, **50**, 15995–15998.

28 E. Bae and W. Choi, *J. Phys. Chem. B*, 2006, **110**, 14792–14799.

29 F. Lakadamyali, M. Kato and E. Reisner, *Faraday Discuss.*, 2012, **155**, 191–205.

30 J. Willkomm, K. L. Orchard, A. Reynal, E. Pastor, J. R. Durrant and E. Reisner, *Chem. Soc. Rev.*, 2016, **45**, 9–23.

31 C. Queffélec, M. Petit, P. Janvier, D. A. Knight and B. Bujoli, *Chem. Rev.*, 2012, **112**, 3777–3807.

32 F. Lakadamyali and E. Reisner, *Chem. Commun.*, 2011, **47**, 1695–1697.

33 N. M. Muresan, J. Willkomm, D. Mersch, Y. Vaynzof and E. Reisner, *Angew. Chem., Int. Ed.*, 2012, **51**, 12749–12753.

34 E. Reisner, J. C. Fontecilla-Camps and F. A. Armstrong, *Chem. Commun.*, 2009, 550–552.

35 S. Morra, F. Valetti, S. J. Sadeghi, P. W. King, T. Meyer and G. Gilardi, *Chem. Commun.*, 2011, **47**, 10566–10568.

36 Z. Chen, J. J. Concepcion, J. W. Jurss and T. J. Meyer, *J. Am. Chem. Soc.*, 2009, **131**, 15580–15581.

37 G. Boschloo and D. Fitzmaurice, *J. Electrochem. Soc.*, 2000, **147**, 1117–1123.

38 B. O'Regan, M. Grätzel and D. Fitzmaurice, *J. Phys. Chem.*, 1991, **95**, 10525–10528.

39 B. O'Regan, M. Grätzel and D. Fitzmaurice, *Chem. Phys. Lett.*, 1991, **183**, 89–93.

40 G. Neri, J. J. Walsh, C. Wilson, A. Reynal, J. Y. C. Lim, X. Li, A. J. P. White, N. J. Long, J. R. Durrant and A. J. Cowan, *Phys. Chem. Chem. Phys.*, 2015, **17**, 1562–1566.

41 A. Reynal, E. Pastor, M. A. Gross, S. Selim, E. Reisner and J. R. Durrant, *Chem. Sci.*, 2015, **6**, 4855–4859.

42 F. Lakadamyali, M. Kato, N. M. Muresan and E. Reisner, *Angew. Chem., Int. Ed.*, 2012, **51**, 9381–9384.

43 D. W. Wakerley and E. Reisner, *Energy Environ. Sci.*, 2015, **8**, 2283–2295.

44 J. Seo, R. T. Pekarek and M. J. Rose, *Chem. Commun.*, 2015, **51**, 13264–13267.

45 A. K. Das, M. H. Engelhard, R. M. Bullock and J. A. S. Roberts, *Inorg. Chem.*, 2014, **53**, 6875–6885.

46 P. D. Tran, A. Le Goff, J. Heidkamp, B. Jousselme, N. Guillet, S. Palacin, H. Dau, M. Fontecave and V. Artero, *Angew. Chem., Int. Ed.*, 2011, **50**, 1371–1374.

47 A. Paracchino, V. Laporte, K. Sivula, M. Grätzel and E. Thimsen, *Nat. Mater.*, 2011, **10**, 456–461.

48 B. Seger, T. Pedersen, A. B. Laursen, P. C. K. Vesborg, O. Hansen and I. Chorkendorff, *J. Am. Chem. Soc.*, 2013, **135**, 1057–1064.

49 N. P. Dasgupta, C. Liu, S. Andrews, F. B. Prinz and P. Yang, *J. Am. Chem. Soc.*, 2013, **135**, 12932–12935.

50 Y.-H. Lai, H. S. Park, J. Z. Zhang, P. D. Matthews, D. S. Wright and E. Reisner, *Chem.–Eur. J.*, 2015, **21**, 3919–3923.

51 J. Zhao, T. Minegishi, L. Zhang, M. Zhong, Gunawan, M. Nakabayashi, G. Ma, T. Hisatomi, M. Katayama, S. Ikeda, N. Shibata, T. Yamada and K. Domen, *Angew. Chem., Int. Ed.*, 2014, **53**, 11808–11812.

52 R. Brimblecombe, A. Koo, G. C. Dismukes, G. F. Swiegers and L. Spiccia, *J. Am. Chem. Soc.*, 2010, **132**, 2892–2894.

53 D. L. Ashford, A. M. Lapides, A. K. Vannucci, K. Hanson, D. A. Torelli, D. P. Harrison, J. L. Templeton and T. J. Meyer, *J. Am. Chem. Soc.*, 2014, **136**, 6578–6581.

54 G. F. Moore, J. D. Blakemore, R. L. Milot, J. F. Hull, H. Song, L. Cai, C. A. Schmuttenmaer, R. H. Crabtree and G. W. Brudvig, *Energy Environ. Sci.*, 2011, **4**, 2389–2392.

55 X. Chen, X. Ren, Z. Liu, L. Zhuang and J. Lu, *Electrochem. Commun.*, 2013, **27**, 148–151.

56 M. de Respinis, K. S. Joya, H. J. M. De Groot, F. D'Souza, W. A. Smith, R. van de Krol and B. Dam, *J. Phys. Chem. C*, 2015, **119**, 7275–7281.

57 K. S. Joya, N. Morlanés, E. Maloney, V. Rodionov and K. Takanabe, *Chem. Commun.*, 2015, **51**, 13481–13484.

58 W. A. Gerrard, *J. Electroanal. Chem.*, 1978, **86**, 421–424.

59 K. L. Hardee and A. J. Bard, *J. Electrochem. Soc.*, 1976, **123**, 1024–1026.

60 T. W. Kim and K.-S. Choi, *Science*, 2014, **343**, 990–994.

61 L. Zhang, C.-Y. Lin, V. K. Valev, E. Reisner, U. Steiner and J. J. Baumberg, *Small*, 2014, **10**, 3970–3978.

62 Q. Mi, A. Zhanaidarova, B. S. Brunschwig, H. B. Gray and N. S. Lewis, *Energy Environ. Sci.*, 2012, **5**, 5694–5700.

63 Y.-H. Lai, T. C. King, D. S. Wright and E. Reisner, *Chem.–Eur. J.*, 2013, **19**, 12943–12947.

64 Y. Belabassi, S. Alzghari and J.-L. Montchamp, *J. Organomet. Chem.*, 2008, **693**, 3171–3178.

65 J. C. Hill and K.-S. Choi, *J. Phys. Chem. C*, 2012, **116**, 7612–7620.

66 Y.-H. Lai, M. Kato, D. Mersch and E. Reisner, *Faraday Discuss.*, 2014, **176**, 199–211.

67 N. Kaeffer, A. Morozan and V. Artero, *J. Phys. Chem. B*, 2015, **119**, 13707–13713.

68 Y.-H. Lai, D. W. Palm and E. Reisner, *Adv. Energy Mater.*, 2015, **5**, 1501668.

69 V. Artero and M. Fontecave, *Chem. Soc. Rev.*, 2013, **42**, 2338–2356.

70 D. Hong, S. Mandal, Y. Yamada, Y.-M. Lee, W. Nam, A. Llobet and S. Fukuzumi, *Inorg. Chem.*, 2013, **52**, 9522–9531.

71 C. Wombwell and E. Reisner, *Dalton Trans.*, 2014, **43**, 4483–4493.

72 N. Zaman, R. Guillot, K. Sénéchal-David and M.-L. Boillot, *Tetrahedron Lett.*, 2008, **49**, 7274–7275.